2D robotic control of a planar dielectrophoresis-based system

Mohamed Kharboutly[1] Alexandre Melis[1], Aude Bolopion[1],
Nicolas Chaillet[1] , *Member, IEEE,* Michaël Gauthier[1] , *Member, IEEE,*

***Abstract*— Nanosciences have recently proposed a lot of proofs of concept of innovative nanocomponents and especially nanosensors. Going from the current proofs of concept on this scale to reliable industrial systems requires the emergence of a new generation of manufacturing methods able to move, position and sort micro-nano-components. We propose to develop 'No Weight Robots-NWR' that use non-contact transmission of movement (e.g. dielectrophoresis, magnetophoresis) to manipulate micro-nano-objects which could enable simultaneous high throughput and high precision. This paper focuses on developing a $2D$ robotic control of the trajectory of a micro-object manipulated by a dielectrophoresis system. A $2D$ dynamic model is used to establish an open loop control law by a numerical inversion. Exploiting this control law, a high speed trajectory tracking (10 Hz) and high precision positioning can be achieved. Several simulated and experimental results are shown to evaluate this control strategy and discuss its performance.**

I. Introduction

This article deals with the robotic control of a non-contact dielectrophoresis system which can be considered as an original robotic structure compared to the current industrial robot. The first industrial robot UNIMATE [1] based on standard joints was commercialized in 1961 (see figure 1). Nowadays more than one million of robots are in use all over the world. In the 1980's the use of compliant structures in robotics [2] was started to enable high precision positioning making them, at present, the most widely used structure for microscale robots [3], [4]. However, transmission of movement in such robots is obtained via the movements of mechanical parts which largely limits throughput due to inertial effects. In the 2000's, LightWeight Robots [5], [6] have been developed by *KUKA*[7] to reduce robot inertia. However, the impact of inertia is still important in the small scales (micro-nano) where the inertia of the object is highly negligible compared to the one of the robots. We propose to develop robots that use non-contact transmission of movement to manipulate micro-nano-objects. Besides eliminating the inertia of a robotic structure, this approach also eliminates friction and adhesion (between the tweezer and the component) which are highly detrimental to a robot performance and life time.

These 'No Weight Robots' NWR are at the cross-road between parallel robot and current non-contact manipulation. Firstly, NWR consists of moving components by applying forces coming from several physical field sources which have a similar effect to parallel robotics [8], [9] where the platform is moved by several mechanical forces coming from several robotic legs. The use of non-contact forces, rather than mechanical forces, changes the robot design drastically. In this regard, existing robotic approaches cannot be transferred to NWR. Secondly, current non-contact manipulation has been achieved mostly by open loop for object positioning or self-assembly [10-17] . The only exception concerns laser trapping which has been experimented in closed-loop by Arai et al. [16], [17]. However, laser trapping induces forces around tens of picoNewtons limiting the achievable throughput. The dielectrophoresis proposed in this paper generate forces around thousand times higher [18], [19]. Providing robotic control strategies will enable active and reprogrammable trajectory control and guarantee the final position of a manipulated object.

This paper introduces a numerical model of a micro-bead's behavior in a dielectrophoresis system in the next section. The 2D trajectory control based on an inverted model is described in the fourth section and experimental validation is presented in the last section.

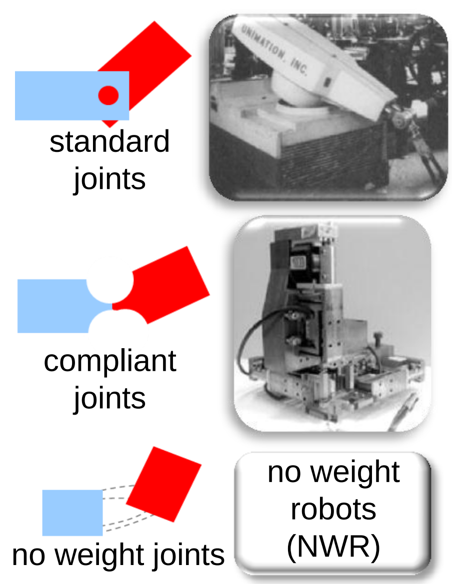

Fig. 1. Movement transmission used in robotics: (i) standard joints used in a majority of robots; (ii) compliant joints based on mechanical deformation used in high precision positionning systems; (iii) the third alternative: movement transmission based on non contact forces

[1] FEMTO-ST Institute, AS2M departement. UMR CNRS 6174 - UFC/ENSMM/UTBM, 24 rue Alain Savary, 25000, Besançon, France, EU.

II. Direct dynamic Model of a dielectrophoresis-based system

In this section, we present a $3D$ dielectrophoretic force simulator applied on a micro-bead, which will be used as reference system. Secondly, a 2D direct dynamic model based on the $3D$ dielectrophoretic force simulator, will be presented and used to establish a 2D control law presented in the next section.

A. Dielectrophoresis force similator

In order to compute the electric field and then the dielectrophoretic force applied to a micro-object in an electrode structure, a numerical simulator is needed. This numerical simulator must be able to compute the dielectrophoretic force generated by very complex geometries in a very short time. For one hand, corresponding analytic equations are very complex and hard to be established. For a second hand, the finite element modeling (FEM) solution is limited to a long computation time and specially when electric voltage changes frequently. Thus, we propose to use the hybrid numeric simulator proposed in [13] gathering the ability of the FEM solution to simulate complex electrodes geometry and the short computation time of the analytical equations. According to [20], the dielectrophoretic force $\overrightarrow{F}_{DEP}$ applied to the micro-bead's center $X(x, y, z)$ with respect to the electric field $\overrightarrow{E}(X, U)$ can be written as:

$$\overrightarrow{F}_{DEP}(X,U) = 2\pi\epsilon_m r^3 Re[K(\omega)]\nabla(\overrightarrow{E}^2(X,U)), \qquad (1)$$

where

$$K(\omega) = \frac{\epsilon_p^* - \epsilon_m^*}{\epsilon_p^* + 2\epsilon_m^*}, \qquad (2)$$

and ϵ_p^* and ϵ_m^* are respectively the complex permittivity of the particle and the medium with:

$$\epsilon^* = \epsilon + j\frac{\sigma}{\omega}, \qquad (3)$$

ϵ is the relative permittivity, σ is the conductivity and ω is the angular velocity of the electric field. Thus, if we consider a configuration of n electrodes, by applying $n-1$ sinusoidal electric voltages identified by there magnitudes $U = [U_1, ...U_{n-1}]$ and there angular velocity ω, the electric field $\overrightarrow{E}(X, U)$ can be computed using the hybrid method described in [13]. This hybrid method consists in computing the electric field $\overrightarrow{E}(X, U)$ by integrating the surface charge density on the electrodes. In fact the electric charge density Q and the magnitudes of the applied voltages U on the electrodes are linearly related:

$$Q = \sum_{i=1}^{n-1}(C_i U_i), \qquad (4)$$

where U_i is the magnitude of the applied voltage on the ith electrode and C_i is the elementary inter-capacitance between the electrodes influenced by the ith electrode. The inter-capacitance between the electrodes depends on only the geometric shape of the electrodes and the electric permittivity of the medium. The C_i is simulated using FEM software. These simulations are executed in preprocessing which reduces the total time of the force computation. If we consider the planar electrodes drawn in the figure 2 (red lines), the number of electrodes n is equal to 4 and they are placed in the x, y plane.

To compute the electric charge density Q with respect to the applied voltages $U = [U_1, U_2, U_3]$, $n - 1 = 3$ FEM simulations are required. The figures 2(a) and 2(b) show the elementary inter-capacitances C_1 and C_3. The figure 2(c) shows how the electric charge density Q is analytically computed with respect to the applied voltages $U = [75V, 0, 75V]$ and the elementary inter-capacitances C_1 and C_3.

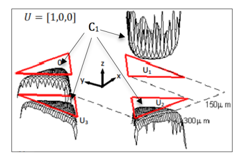

(a) Elementary inter-capacitance C_1.

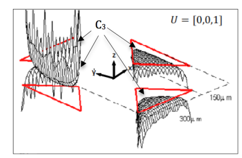

(b) Elementary inter-capacitance C_3.

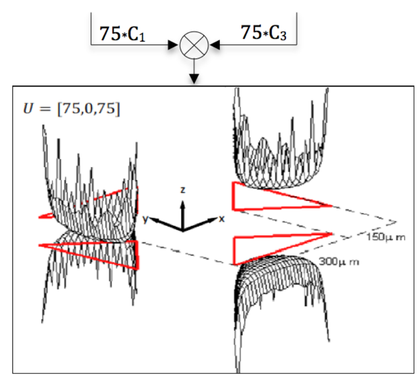

(c) The computed charge density $C = 75 \times C_1 + 75 \times C_3$.

Fig. 2. The electric charge density computed on the electrodes by applying the following electric voltages: $U = [75V, 0, 75V]$.

Once the matrix of the electric charge density Q is computed, the electric field can be calculated analytically in a point $X(x, y, z)$ in the medium. In fact, with each value $Q_{i,j}$ of the computed matrix Q corresponds a $x_{i,j}$, $y_{i,j}$ point on the electrodes ($z_{i,j} = 0$ because of the electrodes are in the x, y plane). Thus, the expression of the electric field $\overrightarrow{E}$ at the point $X(x, y, z)$ is:

$$\overrightarrow{E}(x,y,z) = \sum_i \left(\sum_j \frac{Q_{i,j}\overrightarrow{r}}{4\pi\epsilon_m \|\overrightarrow{r}\|^3} \right), \qquad (5)$$

where $r = [x - x_{i,j}, y - y_{i,j}, z]$, and the DEP force can be also computed analytically with respect to (1). The figure 3 resumes the DEP modeling simulator (DMS) block. The block's inputs are the geometric shape of the electrodes, the applied voltages and the micro-bead's current position. This block generates the computed x, y and z components of the dielectrophoretic force applied to the micro-bead in its center.

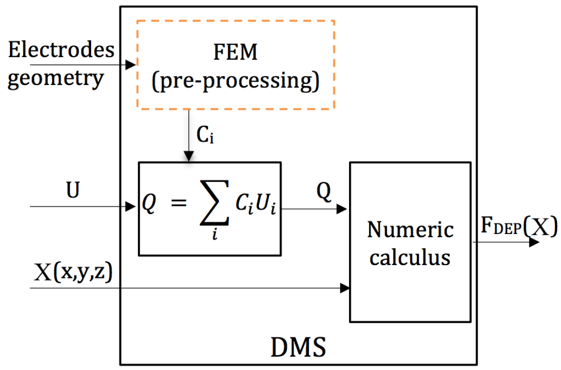

Fig. 3. DEP modeling simulator (DMS).

B. $3D$ direct dynamic model

The dynamic of a micro-bead in motion under dielectrophoretic force field, in a liquid medium is ruled by the following dynamic equation:

$$\overrightarrow{F}_{DEP}(X) + \overrightarrow{F}_{Drag} + \overrightarrow{P} = m\overrightarrow{\ddot{X}}, \quad (6)$$

where X is the space coordinates of the micro-bead's center $X(x, y, z)$, $\dot{X}$ is its velocity, $\ddot{X}$ its acceleration, $\overrightarrow{F}_{DEP}(X)$ is the applied dielectrophoretic force on the center of the micro-bead, $\overrightarrow{P}$ is its apparent weight (sum of the weight and the buoyancy), m is its mass and $\overrightarrow{F}_{Drag}$ is the viscosity friction created on the micro-bead. Generally, in the micro-scale, micro-manipulation in a liquid medium with dynamic viscosity ν is characterized by a Reynolds number much smaller than 1. In this case the micro-bead's inertia impact is very small compared to the viscosity friction $\overrightarrow{F}_{Drag}$. Thus the inertia term $m\overrightarrow{\ddot{X}}$ can be neglected and the dynamic equation becomes:

$$\overrightarrow{F}_{DEP}(X) + \overrightarrow{F}_{Drag}(\dot{X}) + \overrightarrow{P} = 0. \quad (7)$$

In the micron scale the Stokes approach of the viscosity friction is valid, $\overrightarrow{F}_{Drag}(\dot{X})$ becomes:

$$\overrightarrow{F}_{Drag}(\dot{X}) = -6\pi\nu R\overrightarrow{\dot{X}}, \quad (8)$$

where ν is the dynamic viscosity and R the radius of the micro-bead. The dynamic equation is thus:

$$\overrightarrow{\dot{X}} = \frac{\overrightarrow{F}_{DEP}(X) + \overrightarrow{P}}{6\pi\nu R}. \quad (9)$$

The diagram in the figure 4 illustrates the $3D$ direct dynamic modeling. Having the applied electric voltages and the electrodes geometry as input, the direct modeling simulator computes the corresponding micro-bead's trajectory. In generally, the micro-bead's behavior in dielectrophoretic force field is characterized by its high dynamics and nonlinearity. This numeric simulator is experimentally validated in [13] where we have shown that the dynamics are very high and the time response of the micro-bead is less than $3ms$. Moreover the behavior of the micro-bead is subjected to a high nonlinearity and especially when the micro-bead approaches the electrodes.

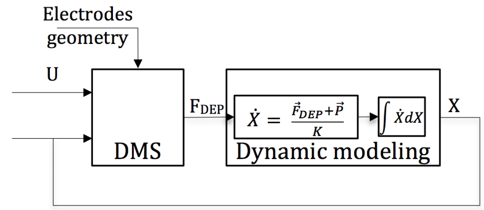

Fig. 4. A dynamic modeling and DMS are used to compute the micro-bead's 3D trajectory.

C. $2D$ simplified dynamic model

In order to reduce the complexity of the computation, we will consider that the electrodes surface is planar in the x, y plane. The $3D$ dielectrophoretic dynamic modeling simulator is designed to run on a classic PC with high performance (typically GHz) and it is not optimized to be integrated directly into a controller card with lower calculation performance (typically MHz). Thus, a reduction of the $3D$ simulator in $2D$ is proposed. We assume that the micro-bead will move only in a $2D$ horizontal plane parallel to the electrodes surface at a height equal to its radius R. The impact of this assumption is going to be discussed at the end of the paper. The $2D$ simulator uses a similar approach to the $3D$ DMS presented above. In this $2D$ model, a database of the elementary spacial force is created. This database links the $2D$ dielectrophoretic force directly to the applied voltages, which will reduce sufficiently the computation time. Using the linear relationship between the electric field $\overrightarrow{E}$ and the applied voltages V, the dielectrophoretic force can be written as a second order equation with respect to the electric voltages. Using the following electric voltages vector (see in figure 5) :

$$V = [-u_y, U_{ref} - u_x, u_y, U_{ref} + u_x]; \quad (10)$$

the $2D$ dielectrophoretic force $[F_{DEP_x},\ F_{DEP_y}]$ can be written as the following:

$$\begin{aligned} F_{DEP_x} &= f_{11}u_x^2 + f_{12}u_y^2 + f_{13}u_x u_y \\ &\quad + f_{14}U_{ref}u_x + f_{15}U_{ref}u_y + f_{16}U_{ref}^2 \\ F_{DEP_y} &= f_{21}u_x^2 + f_{22}u_y^2 + f_{23}u_x u_y \\ &\quad + f_{24}U_{ref}u_x + f_{25}U_{ref}u_y + f_{26}U_{ref}^2. \end{aligned} \quad (11)$$

U_{ref} is a reference voltage, u_x and u_y are the varying voltages and $f_{i,j}$ are spacial functions in x and y essentially dependent on the electrodes geometries. Discrete values of these functions will be computed in a x, y grid points using the $3D$ simulator and stored in a database and a quadratic interpolation is used to evaluate these functions in an arbitrary (x, y) point. Using this $2D$ numeric model, the $2D$ direct dynamic model becomes:

$$\begin{bmatrix} \dot{x} \\ \dot{y} \end{bmatrix} = \frac{1}{6\pi\nu R} \begin{bmatrix} F_{DEP_x} \\ F_{DEP_y} \end{bmatrix} \quad (12)$$

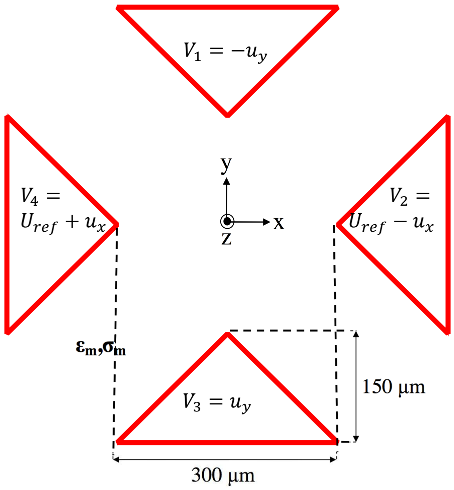

Fig. 5. Geometry of the electrodes and applied voltages: definition of control parameters u_x and u_y.

The weight $\overrightarrow{P}$ has been removed as its projection on the x, y plane is null.

Consequently, the computation time is reduced and few arithmetic iterations are executed in a very short time, even with the interpolation procedure. Indeed, 40 CPU clock cycles are needed to compute the 2 components of the dielectrophoretic force in a grid point, and 180 CPU clock cycle in an interpolated position. In the other hand, using the $3D$ dielectrophoretic force computation, at least 10^4 CPU clock cycle are needed. Thus if we consider that the micro-bead's time response is $3ms$ and for a successful tracking at least 10 control sequence are generated, a controller card with $1MHz$ clock takes $0.2ms$ to compute the dielectrophoretic force using the $2D$ model. The same controller card may takes more then $10ms$ when using the $3D$ dynamic modeling.

III. 2D TRAJECTORY TRACKING

To control the micro-bead's trajectory in a $2D$ dielectrophoretic local periodic structure, an elementary control law for tracking trajectories is presented in this section where a micro-bead moves in one structure. The behavior of a micro-bead in a dielectrophoretic system is characterized by its high dynamics as presented in [13] and the nonlinearity with respect to the applied voltages as shown in the equation (11). This elementary control law must takes into consideration this two problematics. Consequently a simple proportional integrator control is not sufficient especially when the micro-bead approaches the electrodes where the nonlinearity becomes very high. The analytic inversion of the $2D$ model (12) is not possible due to the strong coupling between the control variables u_x and u_y. One way to solve this problem is to use the Newton-Raphson numeric method which is able to find the values of the control variables, u_x and u_y to follow a reference trajectory.

A. $2D$ Inverse dynamic model

Newton-Raphson is a method for finding successively better approximations to the roots of a real-valued functions. By sampling the $2D$ dynamic model (12) and knowing the trajectory $[\hat{x}(t), \hat{y}(t)]$ with respect to the time we are able to compute the appropriate control variable $u_x(t)$ and $u_y(t)$ using the Newton-Raphson method as illustrated in the figure 6:

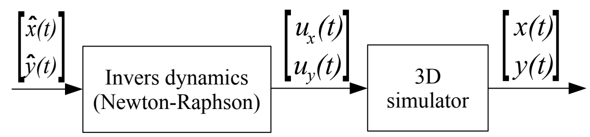

Fig. 6. The Newton-Raphson method is used to find the control variables u_x and u_y

By sampling the dynamic equation (12) using a sampling period T we obtain:

$$\begin{bmatrix} \hat{x}_{k+1} \\ \hat{y}_{k+1} \end{bmatrix} = \frac{T}{6\pi\nu R} \begin{bmatrix} F_{DEP_x}(u_{xk}, u_{y_k}) \\ F_{DEP_y}(u_{xk}, u_{y_k}) \end{bmatrix} + \begin{bmatrix} x_k \\ y_k \end{bmatrix} \quad (13)$$

where $\hat{x}_{k+1}$ and $\hat{y}_{k+1}$ are the next trajectory point at the date kT. Applying the Newton-Raphson method to this model consists in finding iteratively a series of u_x and u_y. At the date kT we have:

$$\begin{bmatrix} u_{x_{k+1}} \\ u_{y_{k+1}} \end{bmatrix} = \begin{bmatrix} u_{x_k} \\ u_{y_k} \end{bmatrix} - J(u_{x_k}, u_{y_k})^{-1} \begin{bmatrix} F(u_{x_k}, u_{y_k}) \\ G(u_{x_k}, u_{y_k}) \end{bmatrix}$$

where u_{x_0} and u_{y_0} are the last computed control variable, J is the jacobin matrix:

$$J(u_{x_k}, u_{y_k}) = \begin{bmatrix} \left.\frac{\partial F(u_x,u_y)}{\partial u_x}\right|_{u_{x_k},u_{y_k}} & \left.\frac{\partial F(u_x,u_y)}{\partial u_y}\right|_{u_{x_k},u_{y_k}} \\ \left.\frac{\partial G(u_x,u_y)}{\partial u_x}\right|_{u_{x_k},u_{y_k}} & \left.\frac{\partial G(u_x,u_y)}{\partial u_y}\right|_{u_{x_k},u_{y_k}} \end{bmatrix} \quad (14)$$

and

$$F(u_x, u_y) = F_{DEP_x}(u_x, u_y) - 6\pi\nu R(\hat{x}_{k+1} - x_k)$$
$$G(u_x, u_y) = F_{DEP_y}(u_x, u_y) - 6\pi\nu R(\hat{y}_{k+1} - y_k) \quad (15)$$

The iterations clasically stops when:

$$\|u_{x_{l+1}} - u_{x_l}\| \leqslant \delta_u \quad and \quad \|u_{y_{l+1}} - u_{y_l}\| \leqslant \delta_u$$

where δ_u is an error threshold.

B. Numeric application and experimental results

Considering the electrodes geometry presented in the figure 7 submerged in a ultra pure water, where the trajectory of a micro-bead made of silica will be controlled. The table I contains the numeric values of the system physical parameters.

Firstly, we are tracking a square reference trajectory with $1s$ period, presented in the figure 8(a).

Applying the Newton-Raphson method, a series of u_x and u_y control variables are computed and presented in the

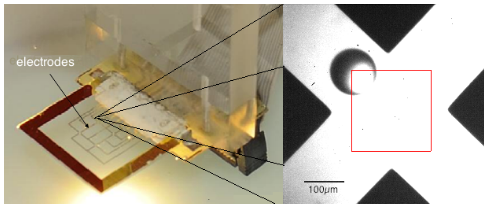

Fig. 7. Experimental electrode used to apply the dielectrophoretic motion. The square presents the reference trajectory.

physical parameters	notations	values
vacuum permittivity	ϵ_0	$8,85 \cdot 10^{-12} CV^{-1}m^{-1}$
particle permittivity	ϵ_p	$8,4 \cdot \epsilon_0$
particle conductivity	σ_p	$10^{-12} Sm^{-1}$
medium permittivity	ϵ_m	$80\epsilon_0$
medium conductivity	σ_m	$4.10^{-6} Sm^{-1}$
water volumlic density	$\mathcal{R}_m$	$1000 Kgm^{-3}$
frequency	f	$10KHz$
Clausius-Mossotti	$Re[K(\omega)]$	-0.42

TABLE I
NUMERICAL APPLICATION

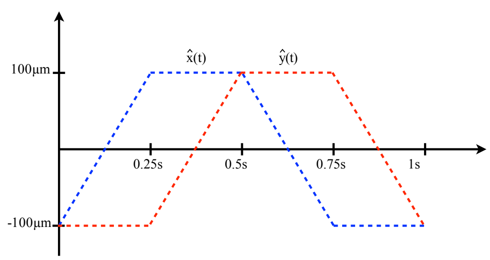

(a) $\hat{x}(t)$ and $\hat{y}(t)$ low speed trajectory.

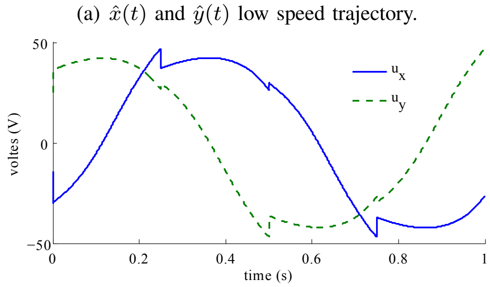

(b) The computed u_x and u_y values for tracking the low speed trajectory.

Fig. 8. The control variable u_x and u_y computed for tracking the low speed trajectory.

figure 8(b). These computed electric voltages are transmitted to a digital-analogic convertor, then they are amplified and applied to the electrodes where the particle is placed (see figure 7). The micro-bead's position is captured by a high speed camera acquisition at 300 images per seconds.

The figure 9 shows the real trajectory of the micro-bead when applying the u_x and u_y series already computed. The relative error between the real trajectory and the reference is less then 8%. This results shows the ability to control the trajectory of a micro-bead in dielectrophoretic system using open loop control strategy.

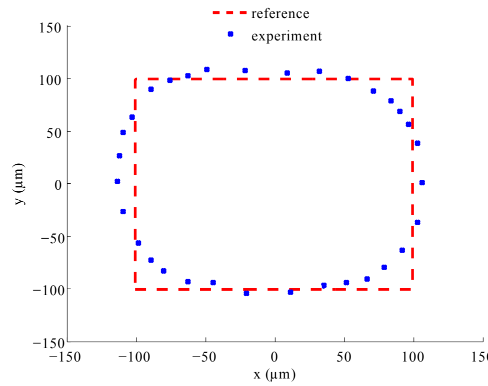

Fig. 9. The real trajectory made by the micro-bead when applying the computed u_x and u_y for the low speed trajectory.

IV. DISCUSSION

In order to show the limitation of our current control law a second experiment with a trajectory 10 times faster is studied (figure 10(a)). The $2D$ controller computes a new series of u_x and u_y presented in the figure 10(b).

The figure 11 shows the real trajectory of the micro-bead when applying the new u_x and u_y series. As this figure shows, the real trajectory does not follow the reference and the error is bigger then 50%. This is essentially due to the limitation of the $2D$ controller where the dynamic model is limited to $2D$.

In reality the micro-bead moves in the three directions x, y and z but in the $2D$ dynamic mode, it supposes to move in a horizontal plane. The main difference between both experiments is the applied voltages u_x and u_y. In the second case, the computed voltage is greater then $50V$. When applying these voltages, experiments show that the height of the micro-beads is significantly different from the plane assumed in the $2D$ dynamic model. Thus, in the first experiment, the real height of the micro-bead is very close to the plane of the $2D$ dynamic modeling consequently the error between the real trajectory and the reference is less then 8%. In the second experiment, the micro-bead's motion is $100\mu m$ higher than the plane of the $2D$ dynamic model, consequently the error between the real trajectory and the reference is bigger then 50%. However, the object trajectory computed using the $3D$ dynamic model is very close to the experimental measurement (see figure 11). This indicates that our $3D$ simulator is reliable and could be used to develop an new $3D$ control law based on a new simplified $3D$ dynamic model.
The current method proposed in this paper has shown its relevance for low altitude trajectories, the extension of this approach in $3D$ will be developed in future works.

V. CONCLUSION

In order to control the trajectory of a micro-object for long distance and high speed, an elementary open-loop positioning control for a micro-bead is presented using dielectrophoresis. A $3D$ dielectrophoretic force simulator

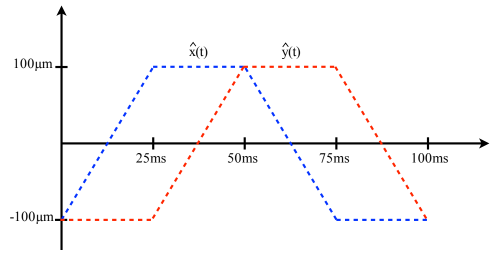

(a) $\hat{x}(t)$ and $\hat{y}(t)$ high speed trajectory.

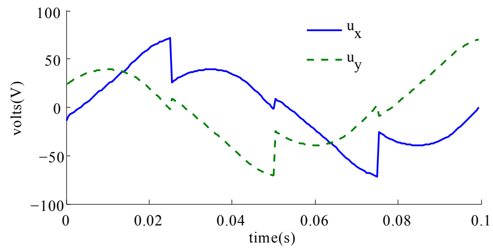

(b) The computed u_x and u_y values for tracking the high speed trajectory.

Fig. 10. The control variable u_x and u_y computed for tracking the high speed trajectory.

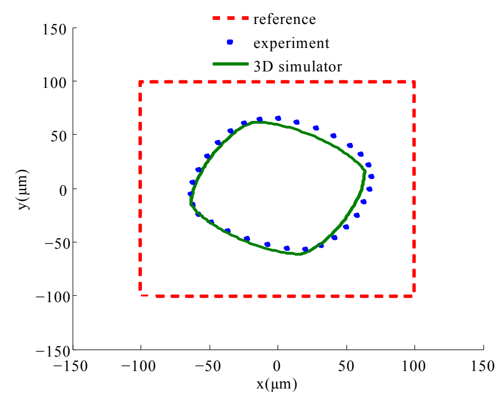

Fig. 11. The real trajectory made by the micro-bead when applying the computed u_x and u_y for the high speed trajectory.

has been firstly presented. We have shown that the full $3D$ dynamic model is too complex to be introduced in a controller card. Thus a reduced $2D$ dynamic model based on the $3D$ dynamic model was developed. This model is then used to establish a $2D$ control law. We have shown that inverting this model cannot be done in an analytic way and we have proposed to use the Newton-Raphson numerical method, in order to compute the appropriate control variable with respect to a reference trajectory. Two experiments was presented including two reference trajectories with different speeds. Experiments have shown that the $2D$ controller has succeeded to track the low speed trajectory, and failed to track the high speed trajectory. This difference has been also discussed. Experiments also have confirmed that the original $3D$ dynamic modeling is reliable, and could be used in developing a new control law dedicated to $3D$ trajectories.

ACKNOWLEDGMENT

The authors would like to thank all the contributors in this collaborative work under the european project FAB2ASM (contract FoF-NMP-2010-260079): Efficient and Precise 3D Integration of Heterogeneous Microsystems from Fabrication to Assembly, (http://fab2asm.eu/). This article is also supported by the european project IRSES EC-NANOMAN, European Chinese exchange program project on Nanomanipulation.

REFERENCES

[1] G. C. Devol, "Programmed article transfer," USA Patent 2 988 237, June 13, 1961.

[2] J. D. Schutter and H. V. Brussel, "Compliant robot motion i. a formalism for specifying compliant motion tasks," *The int. Journal of Robotics Research*, vol. 7, no. 4, pp. 3–17, 1988.

[3] J-P.Bacher, C.Joseph, and R.Clavel, "Flexures for high precision robotics," *Industrial Robot: An international Journal*, vol. 29, no. 4, 2002.

[4] M. Richard and R. Clavel., "Concept of modular flexure-based mechanisms for ultra-high precision robot design," *Mechanical Sciences*, vol. 2, pp. 99–107, 2011.

[5] G. Hirzinger, M. Fischer, B. Brunner, R. Koeppe, M. Otter, M. Grebenstein, and I. Schäfer, "Advances in robotics: The dlr experience," *The International Journal of Robotics Research*, vol. 18, p. 1064, 1999.

[6] G. Schreiber, A. Stemmer, and R. Bischoff, "The fast research interface for the kuka lightweight robot." in *IEEE ICRA 2010 Workshop on Innovative Robot Control Architectures for Demanding (Research) Applications*, Anchorage, May 2010, p. 2010.

[7] KUKA. [Online]. Available: www.kuka-roboter.de

[8] F. Pierrot, V. Nabat, O. Company, S. Krut, and P. Poignet, "Optimal design of a 4-dof parallel manipulator: From academia to industry," *IEEE Transactions onRobotics*, vol. 25, no. 2, pp. 213 – 224, 2009.

[9] S. Bellakehal, N. Andreff, Y. Mezouar, and M. Tadjine, "Force/position control of parallel robots using exteroceptive pose measurements," *Meccanica*, vol. 46, no. 1, pp. 195–205, 2011.

[10] C. Pawashe, S. Floyd, and M. Sitti, "Multiple magnetic microrobot control using electrostatic clamping,," *Applied Physics Letters*, vol. 94, p. 164108, 2009.

[11] S. Floyd, C. Pawashe, and M. Sitti, "Two-dimensional contact and non-contact micro-manipulation in liquid using an untethered mobile magnetic micro-robot," *IEEE Transactions on Robotics*, vol. 25, no. 6, pp. 1332–1342, 2009.

[12] I. Ivan, G. Hwang, J. Agnus, M. Rakotondrabe, N. Chaillet, and S. Regnier, "First experiments on magpier: A planar wireless magnetic and piezoelectric microrobot," in *IEEE International Conference onRobotics and Automation (ICRA)*, 2011, pp. 102 – 108.

[13] M. Kharboutly, M. Gauthier, and N. Chaillet, "Modeling the trajectory of a micro particle in a dielectrophoresis device." *Journal of Appl. Phys.*, vol. 106, no. 11, pp. 114 312 – 114 312–7, 2009.

[14] T. Sun and H. Morgan, "Ac electrokinetic micro- and nano-particle manipulation and characterization," *Electrokinetics and Electrohydrodynamics in Microsystems, CISM Courses and Lectures, Springer*, vol. 530, pp. 1–28, 2011.

[15] A. Kuzyk, "Dielectrophoresis at the nanoscale," *electrophoresis*, vol. 32, no. 17, pp. 2307–2313, 2011.

[16] F. Arai, K. Yoshikawa, T. Sakami, and T. Fukuda, "Synchronized laser micromanipulation of multiple targets along each trajectory by single laser," *Appl. Phys. Lett.*, vol. 85, 2004.

[17] K. Onda and F. Arai, "Multi-beam bilateral teleoperation of holographic optical tweezers," *Optics Express*, vol. 20, no. 4, pp. 3633–3641, 2012.

[18] M. Kharboutly, M. Gauthier, and N. Chaillet, "Modeling the trajectory of a micro particle in a dielectrophoresis device," in *IEEE International Conference on Robotics and Automation ICRA 2010*, Alaska, USA, May 2010.

[19] ——, "Predictive control of a micro bead's trajectory in a dielectrophoresis-based device," in *IEEE/RSJ International Conference on Intelligent Robots and Systems*, Taipei, Taiwan, oct. 2010.

[20] M. P. Hughes, *Nanoelectromechanics in Engineering and Biology*. CRC PRESS, 2002.